Electronic Supplementary Information

Phenylalanine Conjugated Supramolecular Hydrogel Developed from Mafenide and Flurbiprofen Multidrug for Biological Applications

Utsab Manna, Rajdip Roy, Abhishek Dutta, Nabanita Roy*

Address: *School of Chemical Sciences, Indian Association for the Cultivation of Science (IACS), 2A and 2B, Raja S. C. Mullick Road, Jadavpur, Kolkata - 700032, West Bengal, India*
E-mail: utsabmanna1991@gmail.com , csum2487@iacs.res.in,
*Corresponding author

Table of Content

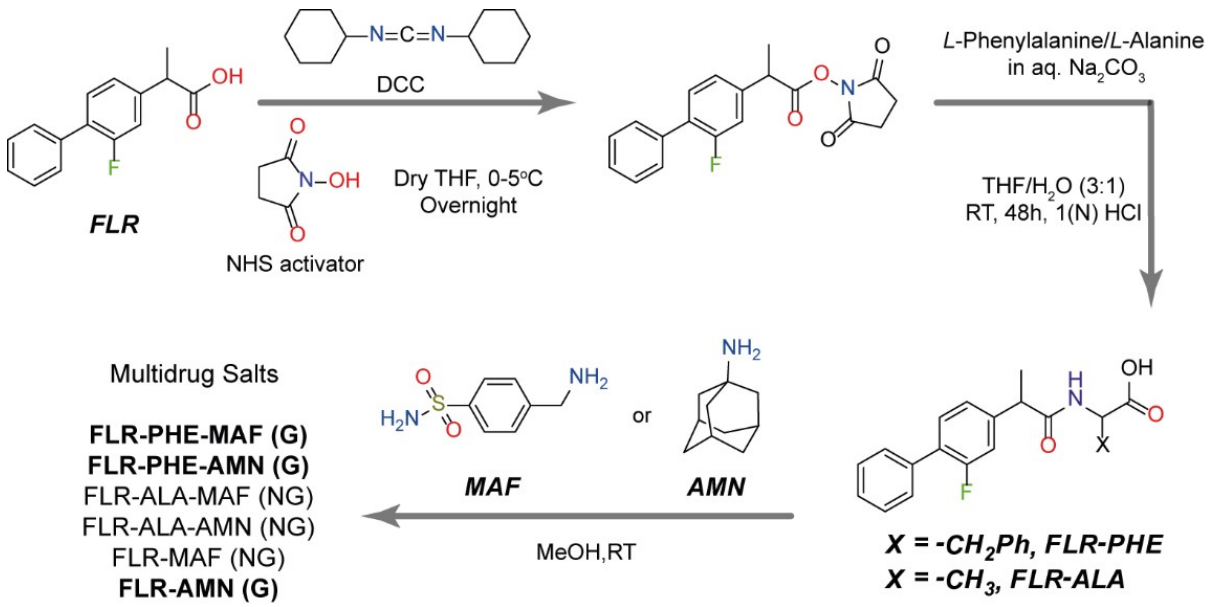

Scheme S1: General synthetic routes for the preparation of various multidrug salts studied herein.

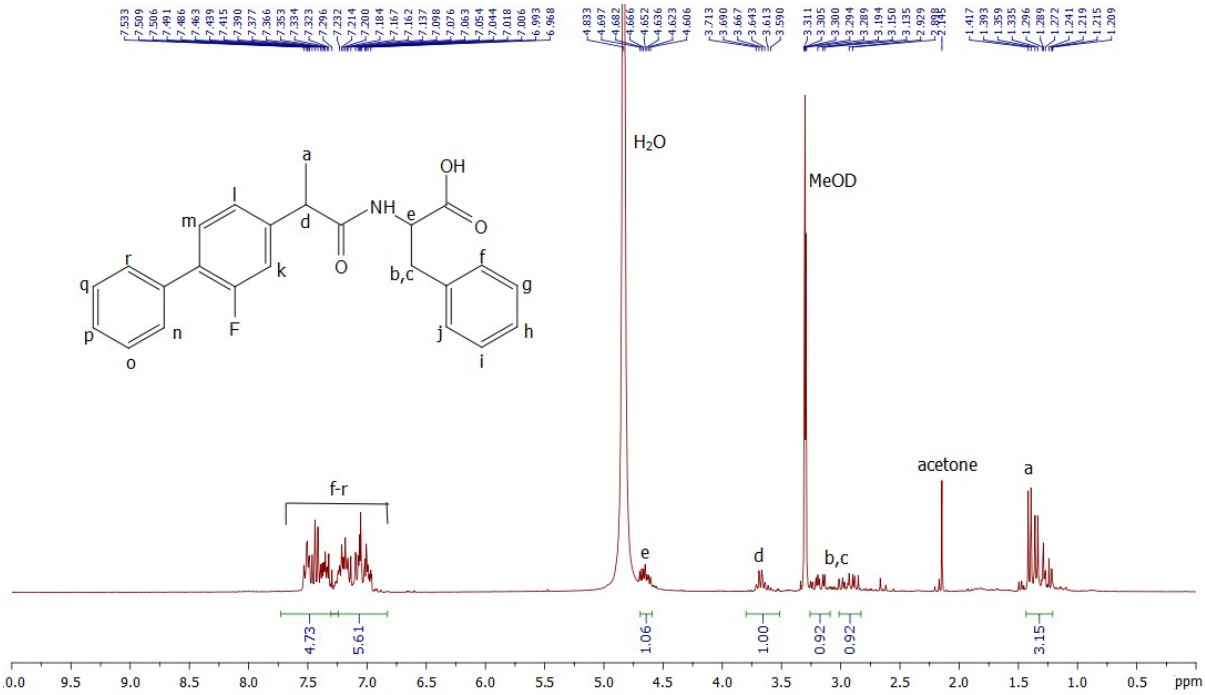

Figure S1: ^{1}H-NMR spectra of **FLR·PHE** acid in MeOD.

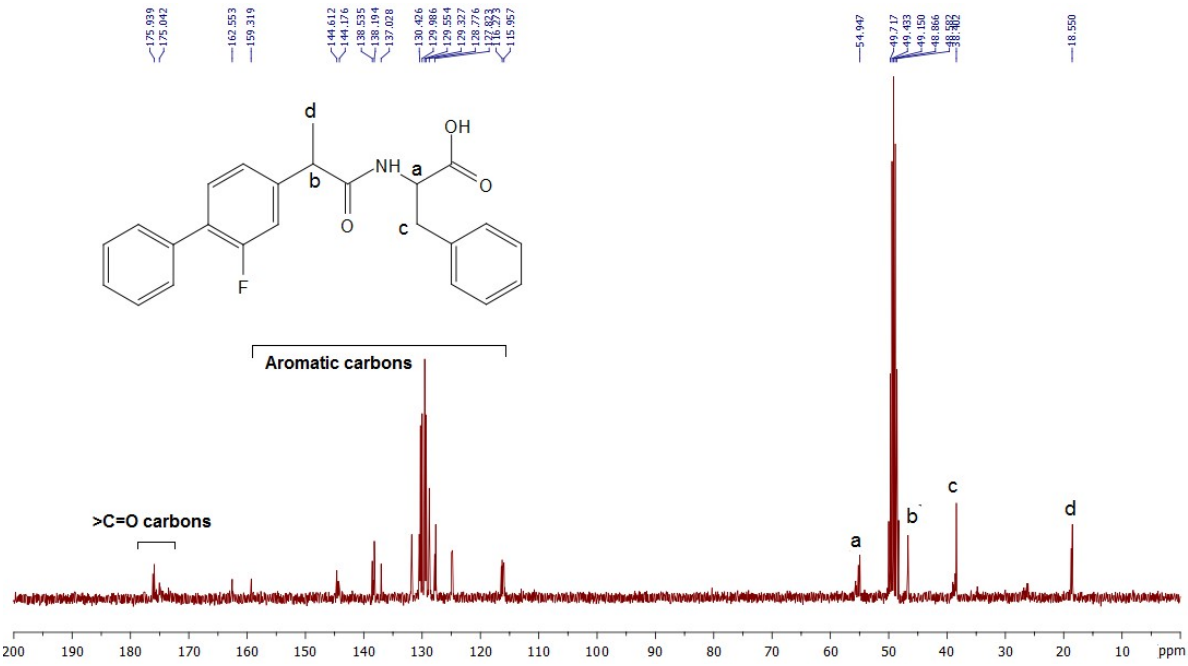

Figure S2: ^{13}C-NMR spectra of **FLR·PHE** acid in MeOD.

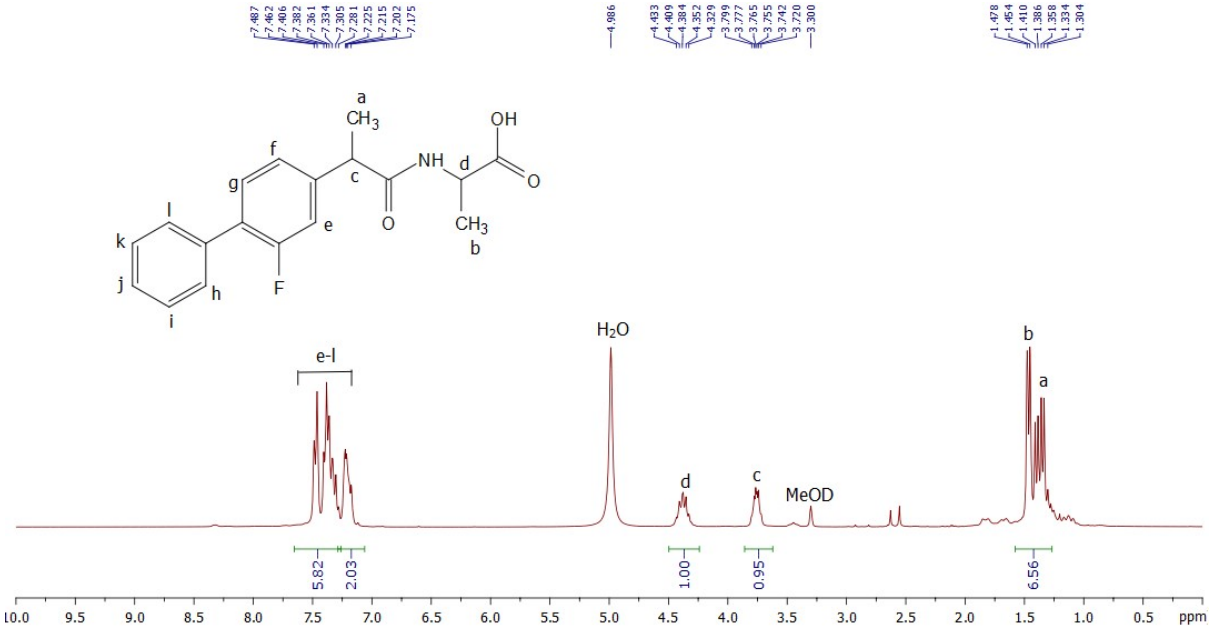

Figure S3: ^{1}H-NMR spectra of **FLR·ALA** acid in MeOD.

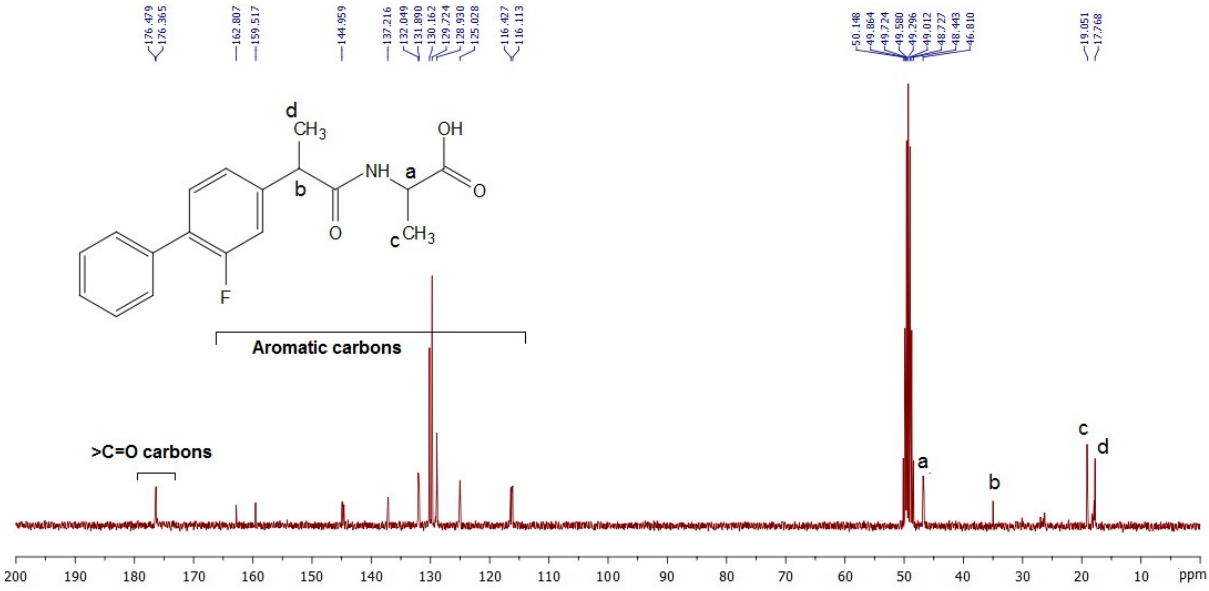

Figure S4: ^{13}C-NMR spectra of **FLR·ALA** acid in MeOD.

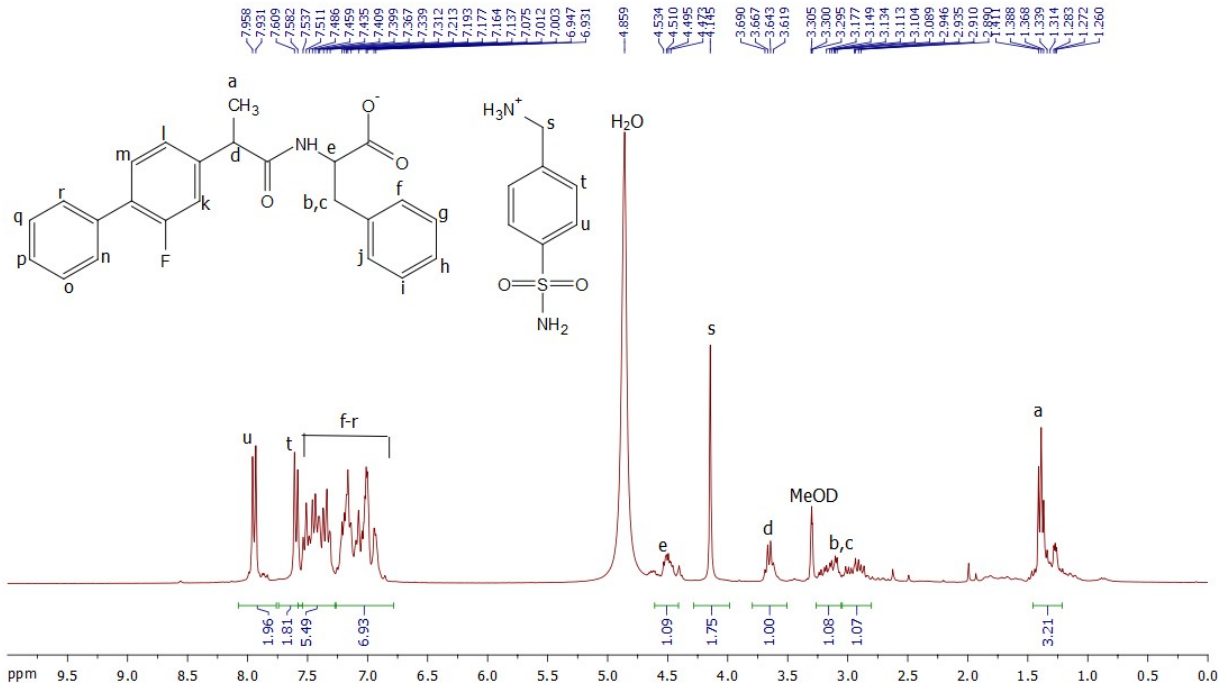

Figure S5: ^{1}H-NMR spectra of multidrug salt **FLR·PHE·MAF** in MeOD.

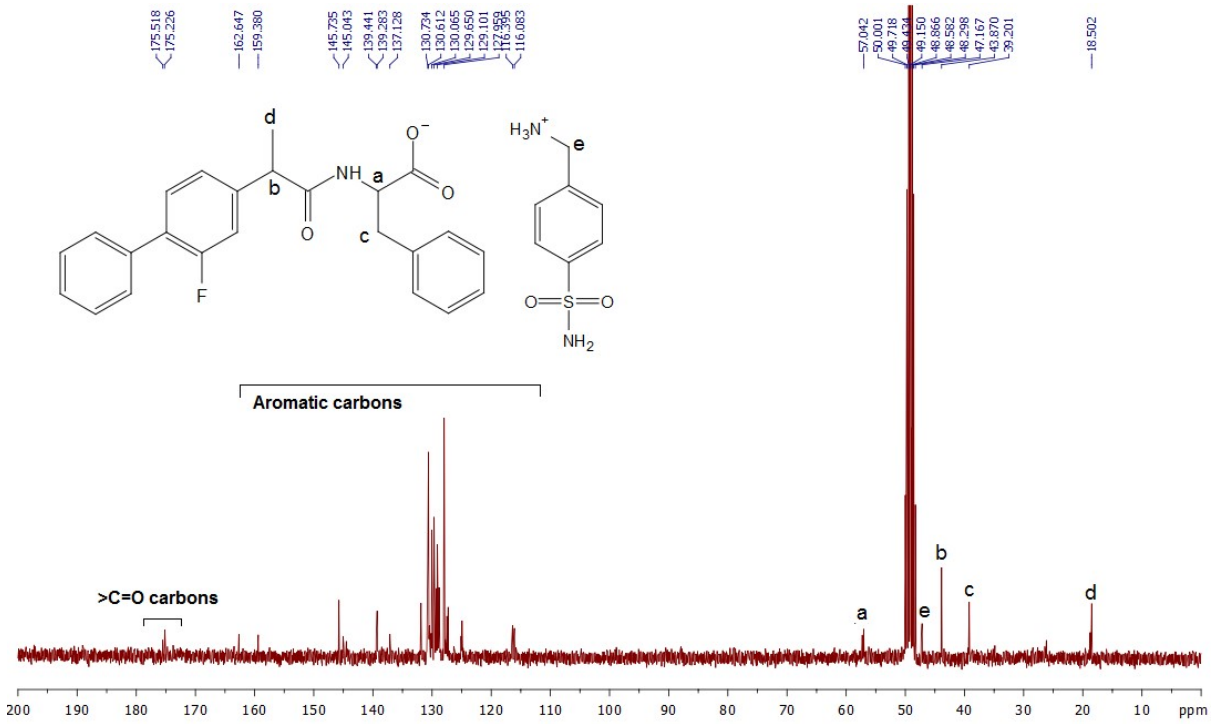

Figure S6: ^{13}C-NMR spectra of multidrug salt **FLR·PHE·MAF** in MeOD.

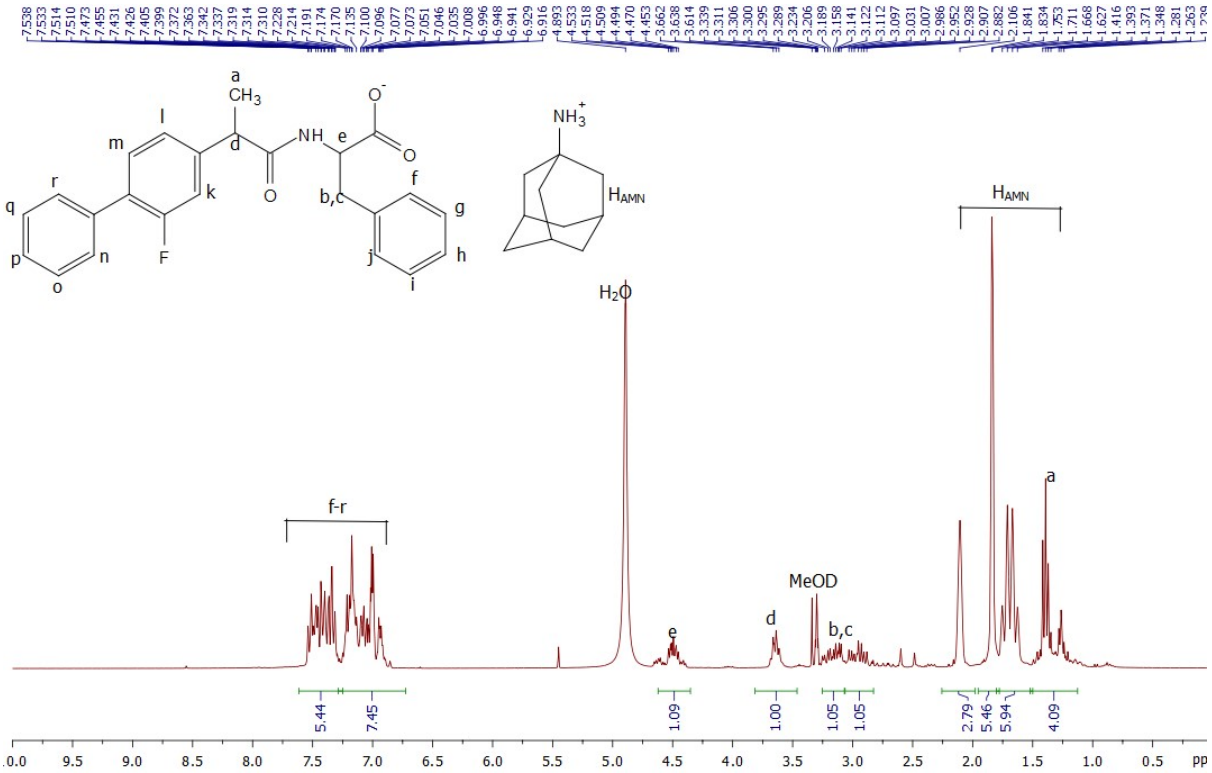

Figure S7: ^{1}H-NMR spectra of multidrug salt **FLR·PHE·AMN** in MeOD.

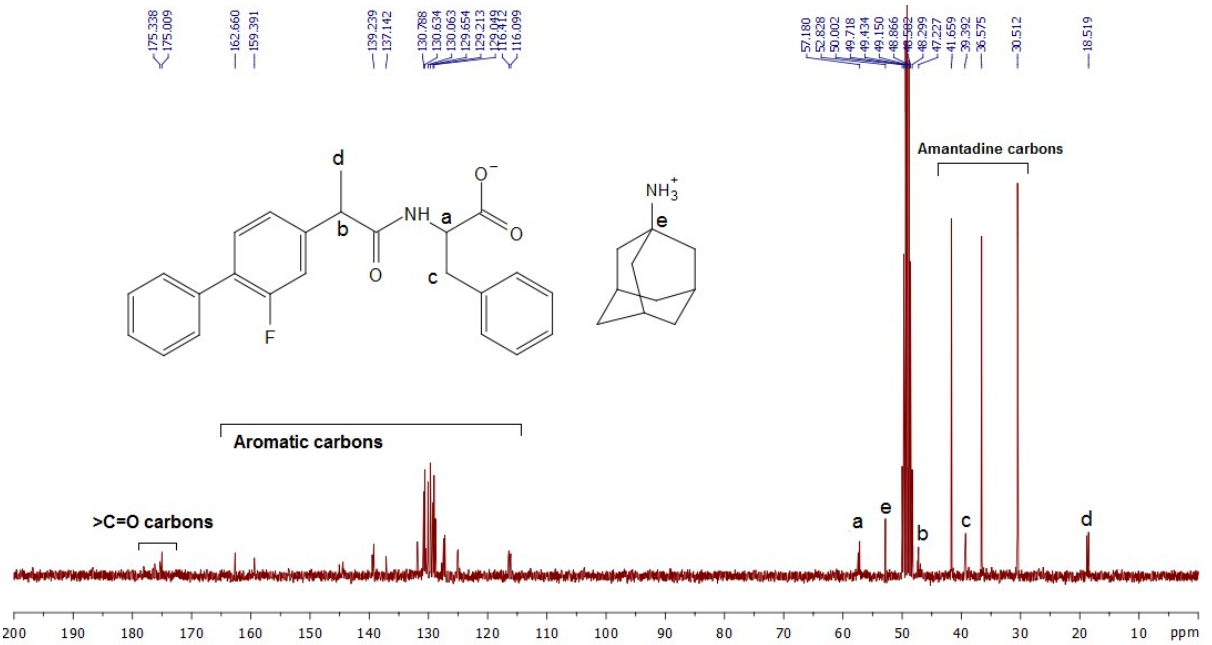

Figure S8: ^{13}C-NMR spectra of multidrug salt **FLR·PHE·AMN** in MeOD.

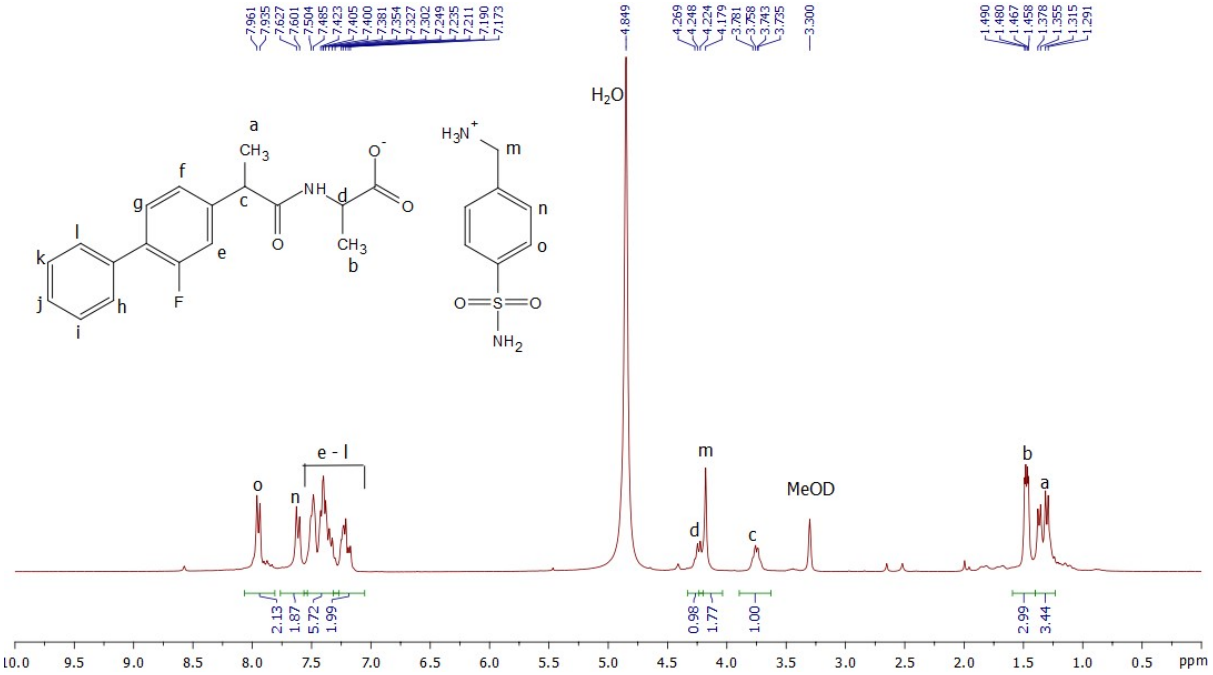

Figure S9: ^{1}H-NMR spectra of multidrug salt **FLR·ALA·MAF** in MeOD.

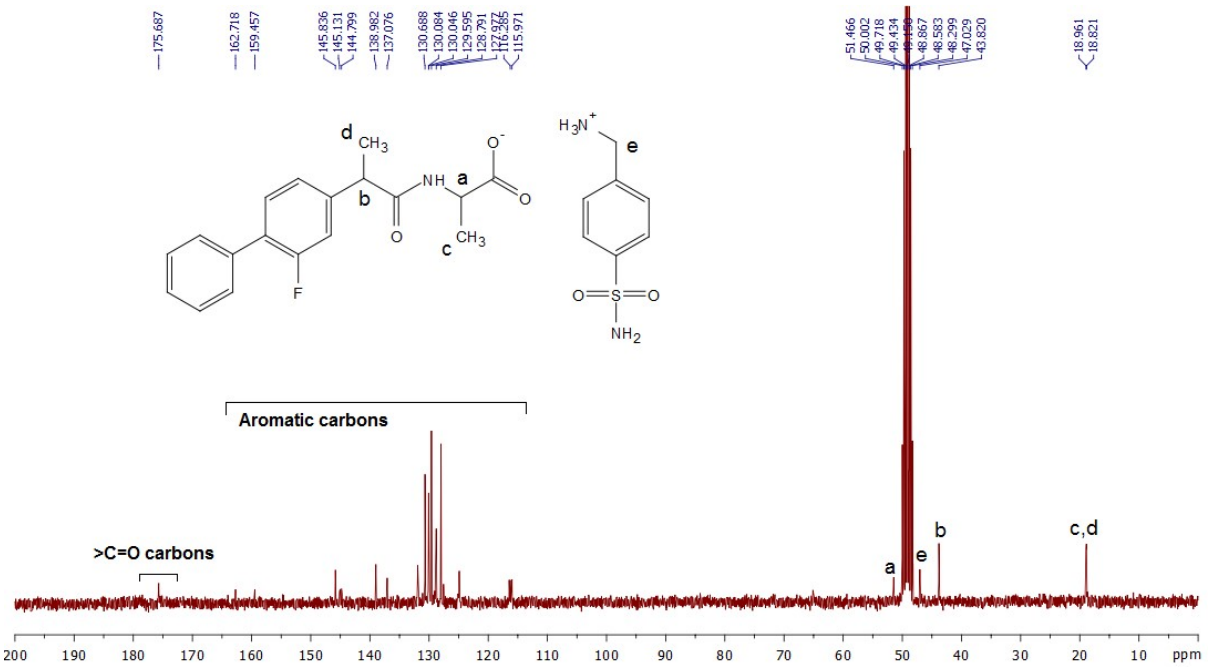

Figure S10: ^{13}C-NMR spectra of multidrug salt **FLR·ALA·MAF** in MeOD.

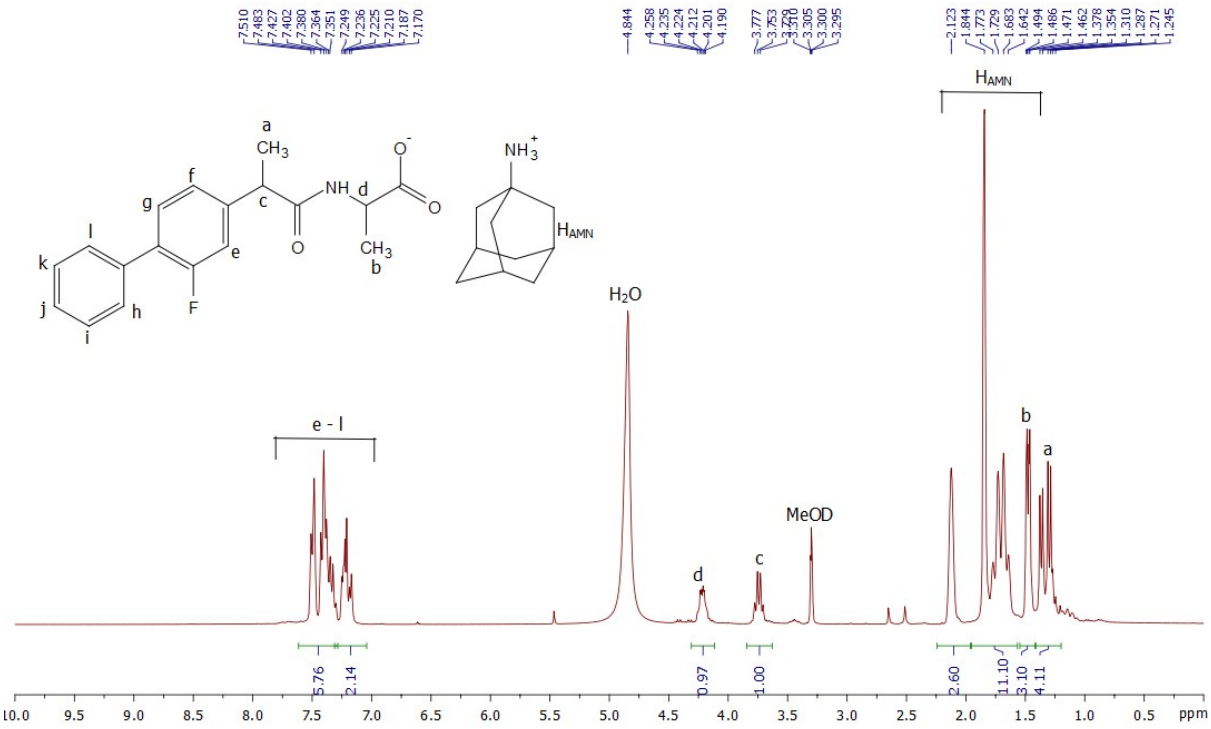

Figure S11: ^{1}H-NMR spectra of multidrug salt **FLR·ALA·AMN** in MeOD.

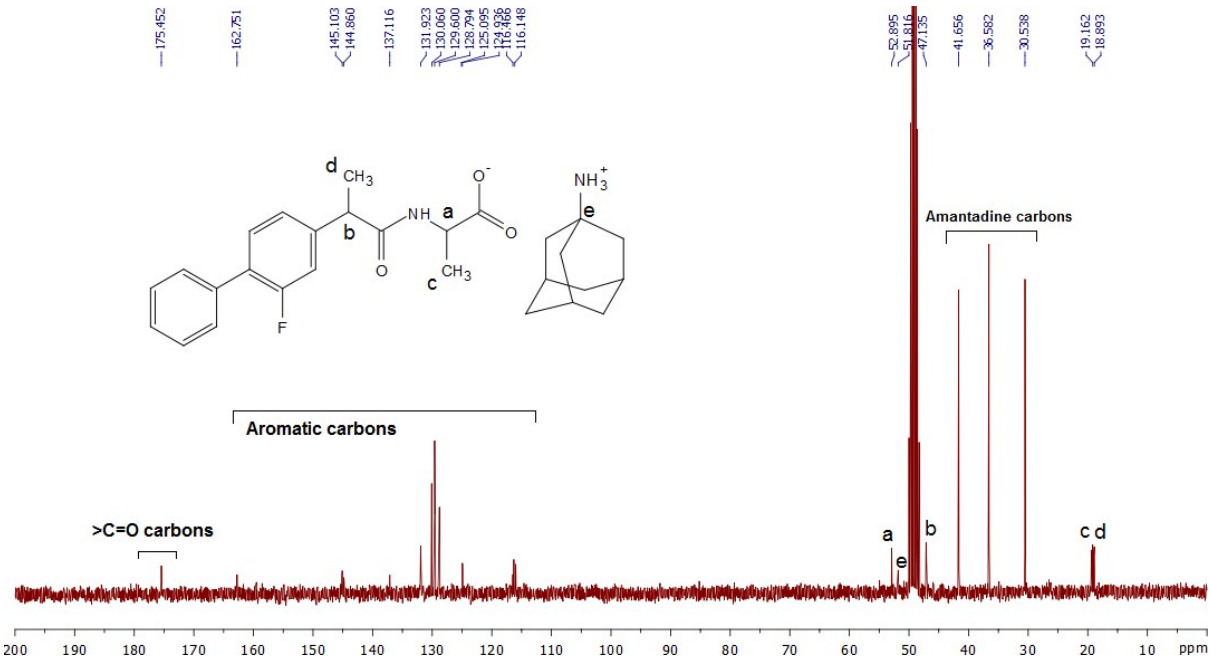

Figure S12: ^{13}C-NMR spectra of multidrug salt **FLR·ALA·AMN** in MeOD.

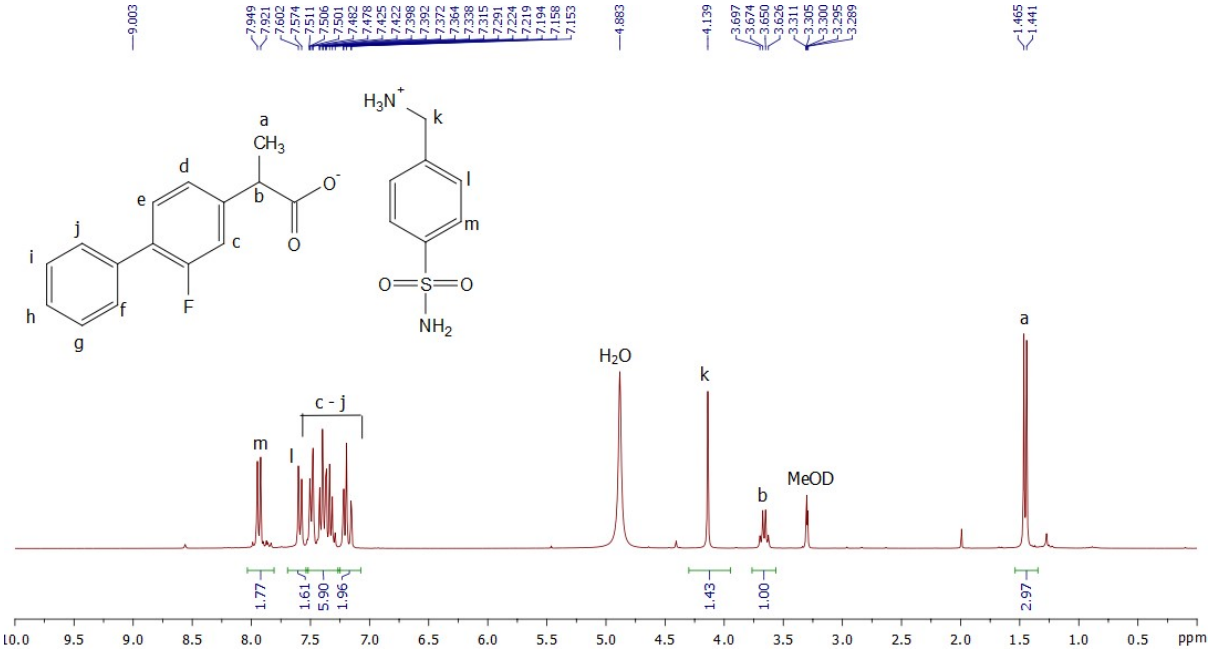

Figure S13: ^{1}H-NMR spectra of multidrug salt **FLR·MAF** in MeOD.

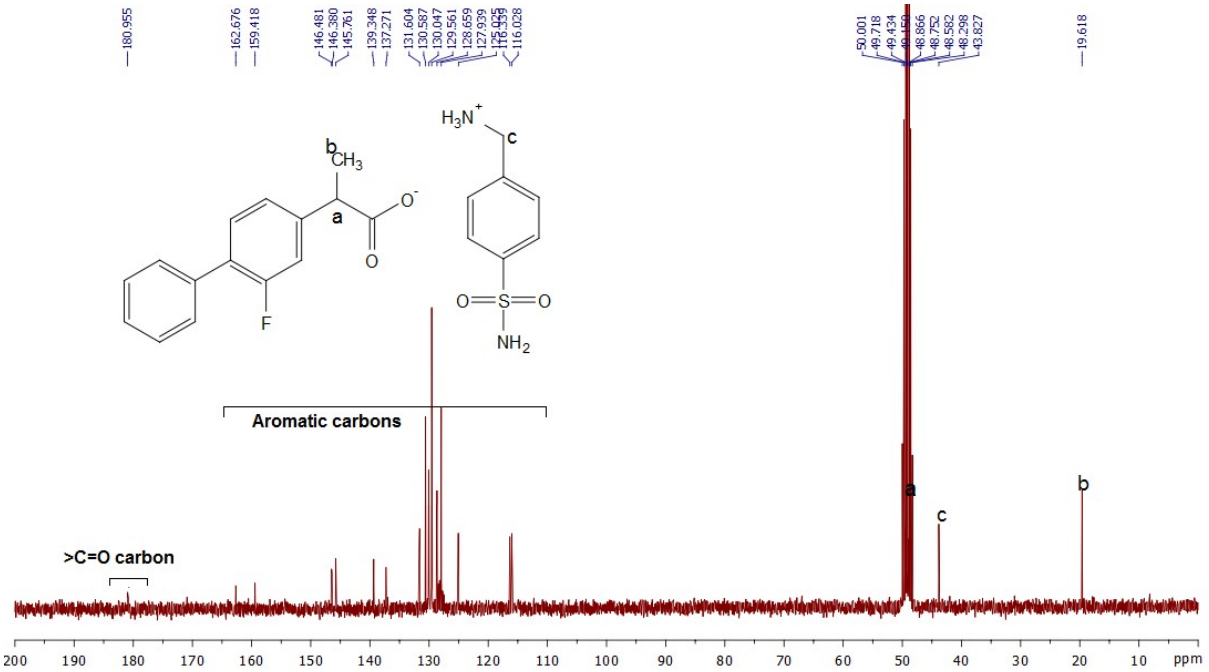

Figure S14: ^{13}C-NMR spectra of multidrug salt **FLR·MAF** in MeOD.

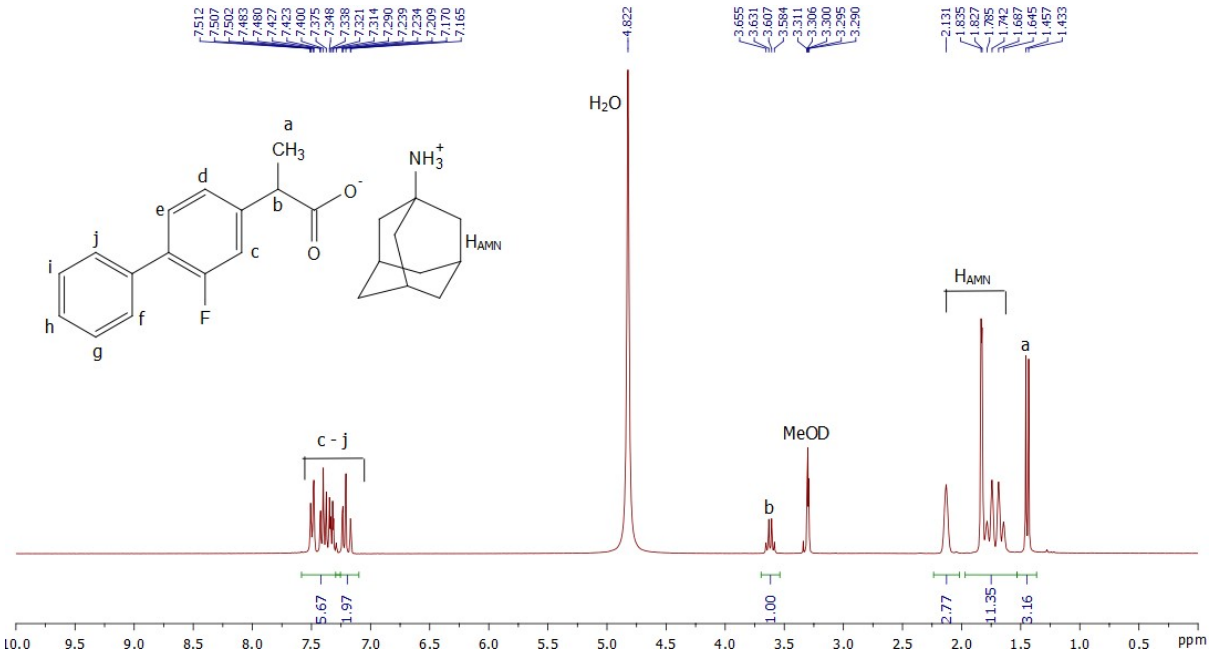

Figure S15: ^{1}H-NMR spectra of multidrug salt **FLR·AMN** in MeOD.

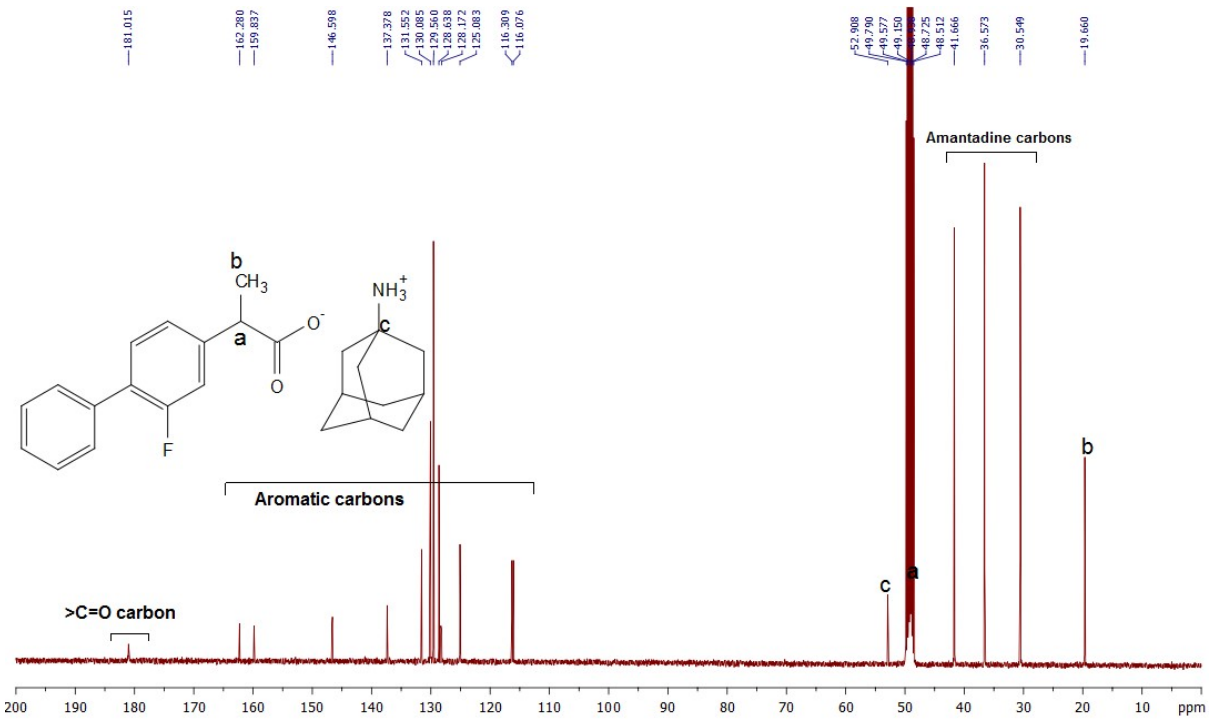

Figure S16: ^{13}C-NMR spectra of multidrug salt **FLR·AMN** in MeOD.

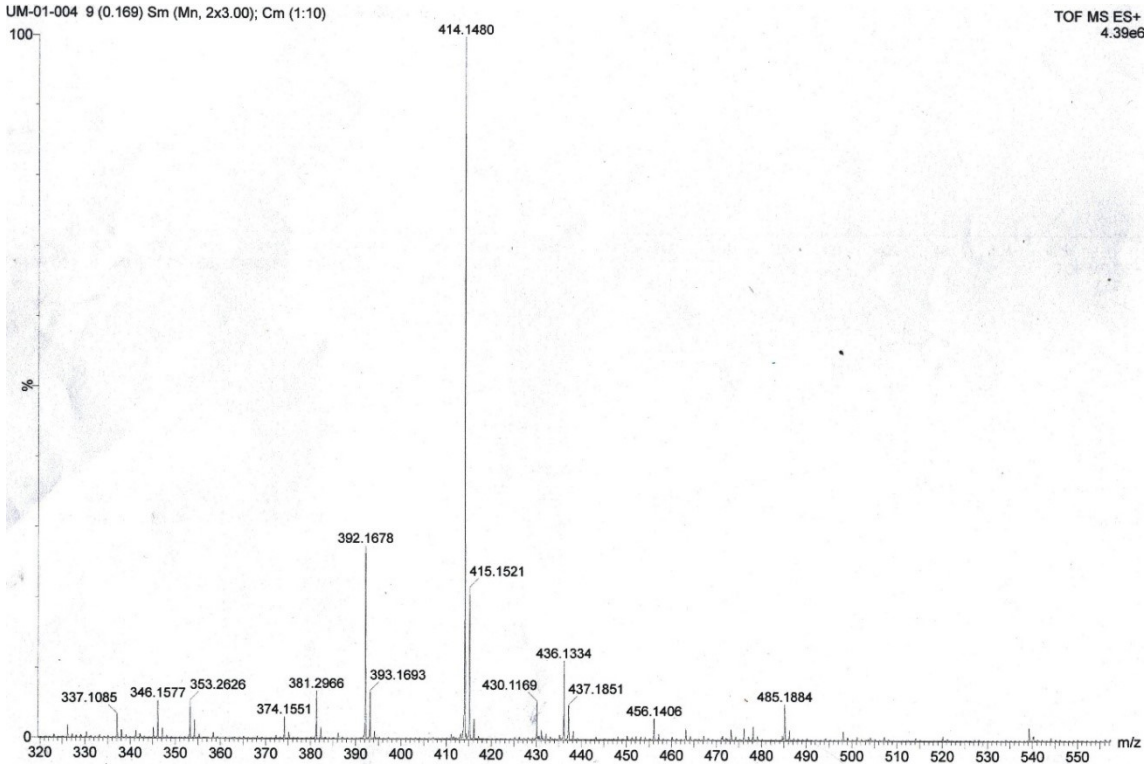

Figure S17: ESI-MS spectra of **FLR·PHE** acid. (MW = 390.4350) HRMS, ESI (CH_3OH) *m/z* (100%): calculated for $[(C_{24}H_{22}FNO_3)][M+Na]^+$: 414.15; found: 414.1480.

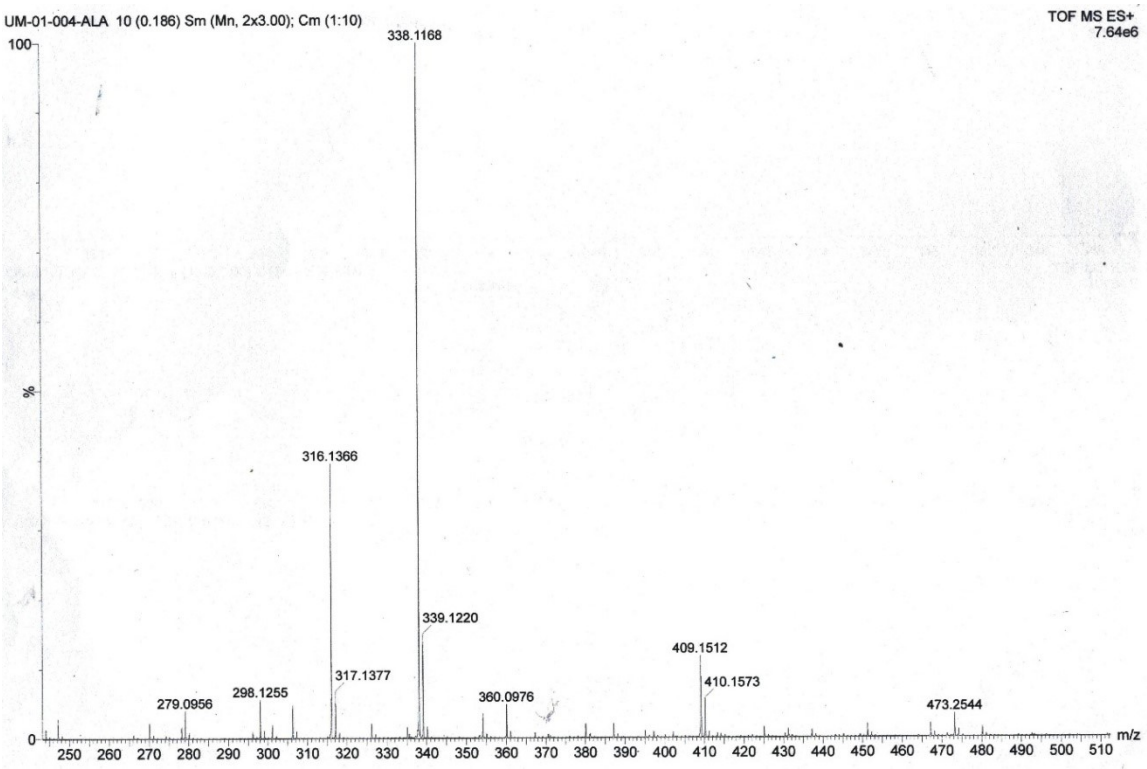

Figure S18: ESI-MS spectra of **FLR·ALA** acid. (MW = 314.3370) HRMS, ESI (CH_3OH) *m/z* (100%): calculated for $[(C_{18}H_{18}FNO_3)][M+Na]^+$: 338.12; found: 338.1168.

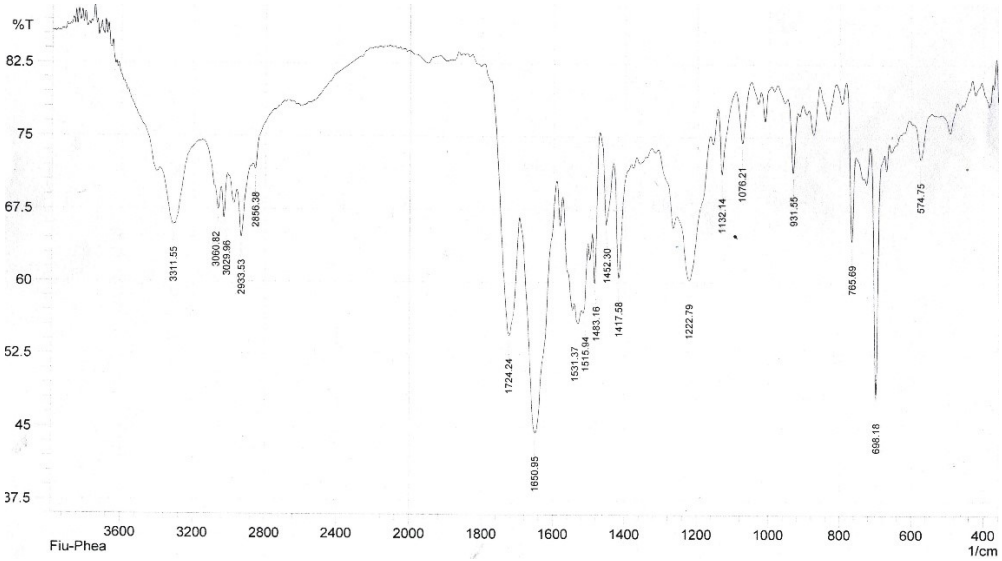

Figure S19: FT-IR spectra of **FLR·PHE** acid. Charcteristic >C=O_{COOH} peak at 1724.24 cm^{-1}.

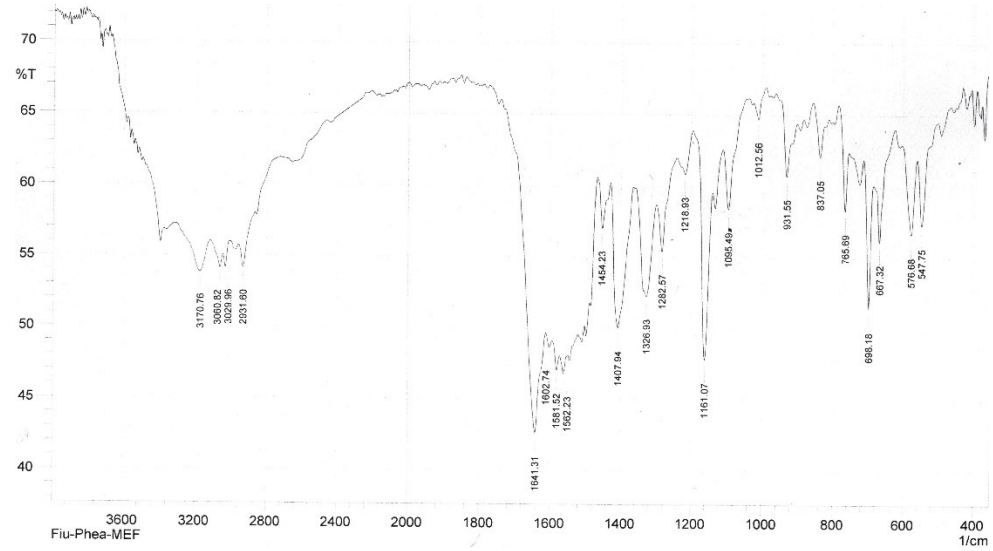

Figure S20: FT-IR spectra of **FLR·PHE·MAF** multidrug salt with the presence of charcteristic >C=O_{COO-} peak at 1641.31 cm^{-1} followed by the absense of >C=O_{COOH} peak.

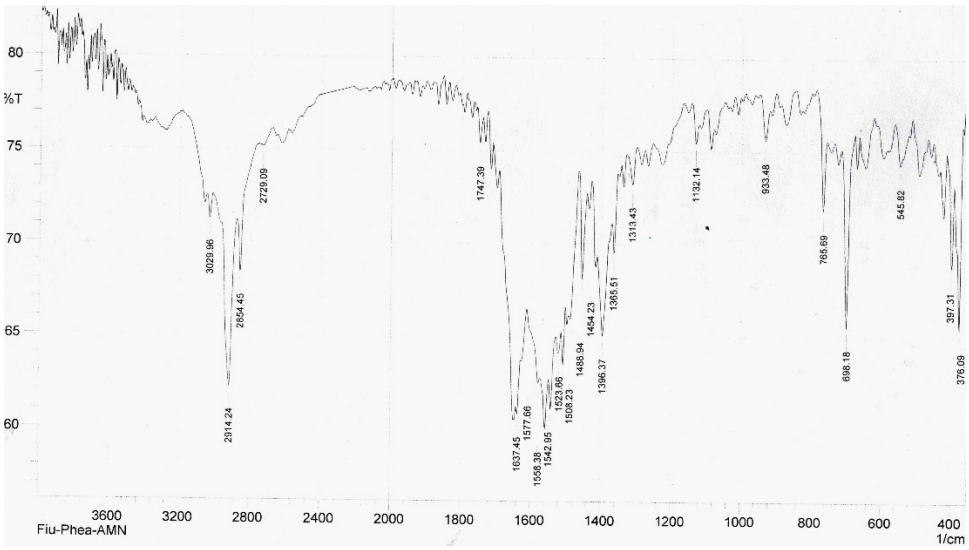

Figure S21: FT-IR spectra of **FLR·PHE·AMN** multidrug salt with the presence of charcteristic >C=O_{COO-} peak at 1637.45 cm^{-1} followed by the absense of >C=O_{COOH} peak.

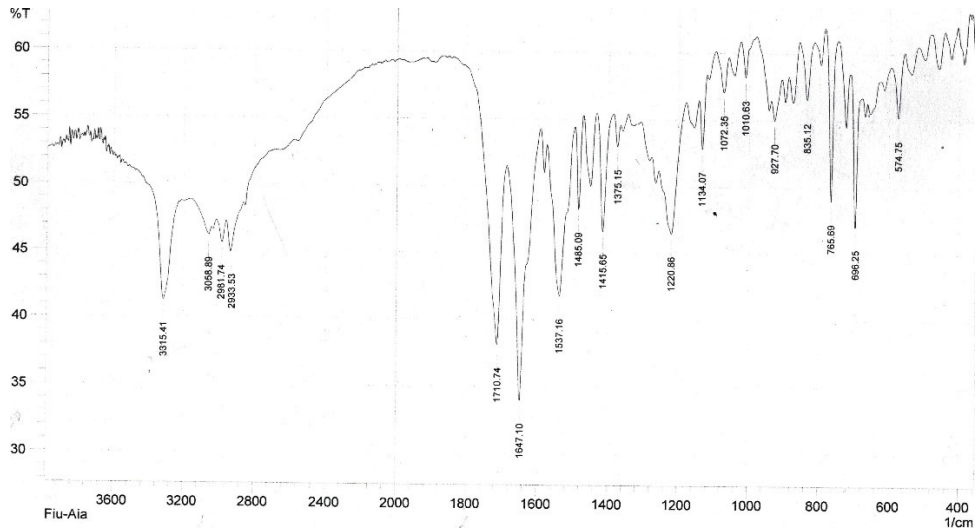

Figure S22: FT-IR spectra of **FLR·ALA** acid. Charcteristic >C=O_{COOH} peak at 1710.74 cm^{-1}.

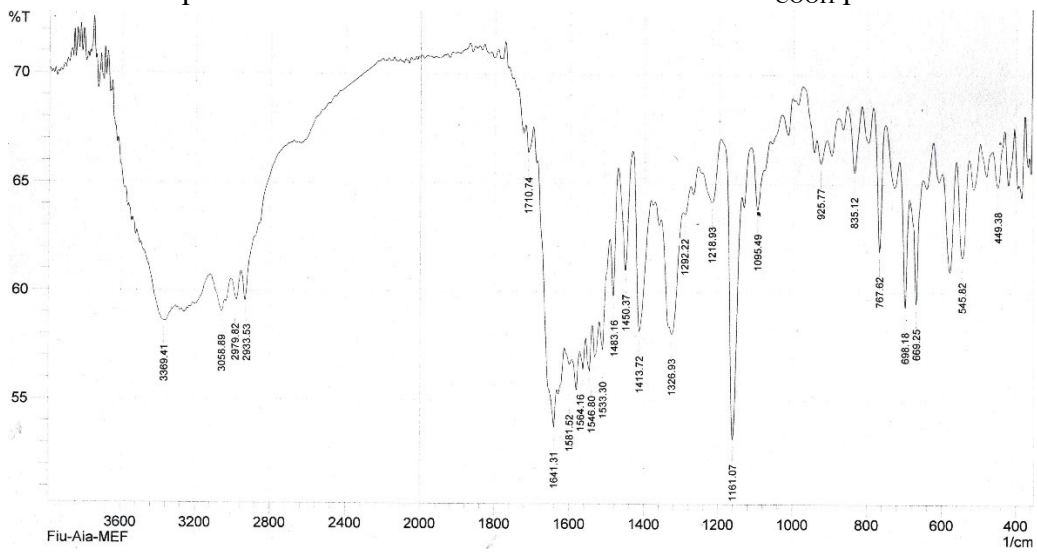

Figure S23: FT-IR spectra of **FLR·ALA·MAF** multidrug salt with the presence of charcteristic >C=O_{COO-} peak at 1641.31 cm^{-1} followed by the absense of >C=O_{COOH} peak.

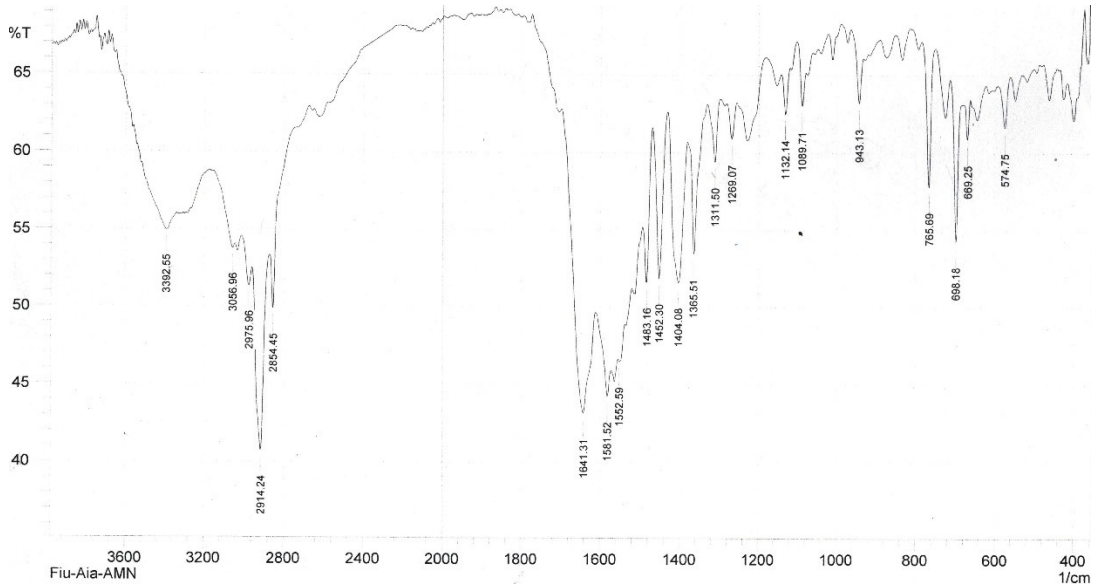

Figure S24: FT-IR spectra of **FLR·ALA·AMN** multidrug salt with the presence of charcteristic >C=O_{COO-} peak at 1641.31 cm^{-1} followed by the absense of >C=O_{COOH} peak.

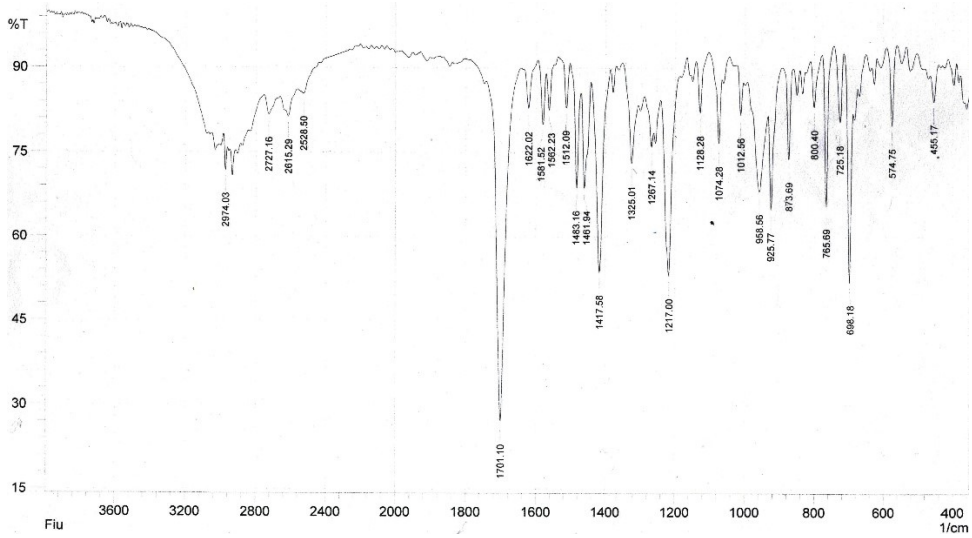

Figure S25: FT-IR spectra of **FLR** acid. Charcteristic >C=O_{COOH} peak at 1701.10 cm^{-1}.

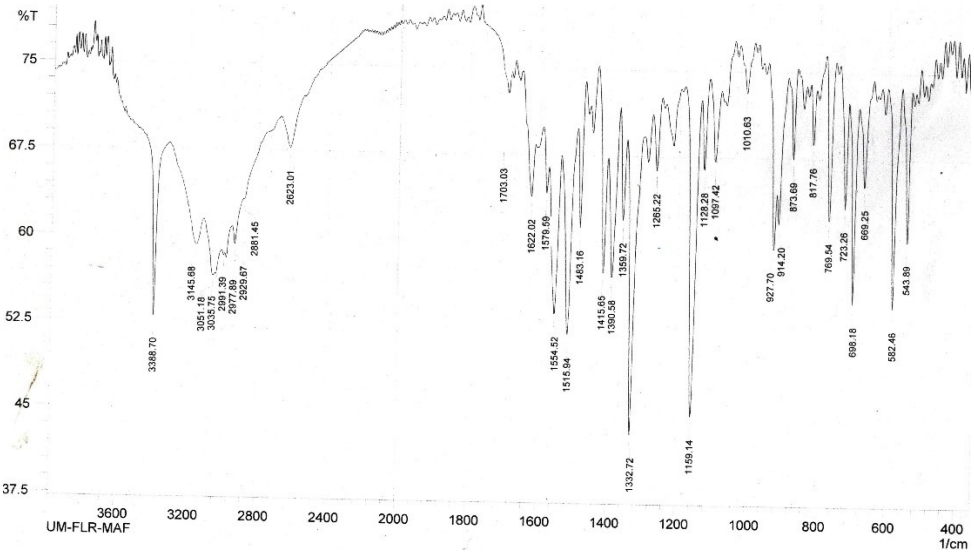

Figure S26: FT-IR spectra of **FLR·MAF** multidrug salt with the presence of charcteristic >C=O_{COO-} peak at 1622.02 cm^{-1} followed by the absense of >C=O_{COOH} peak.

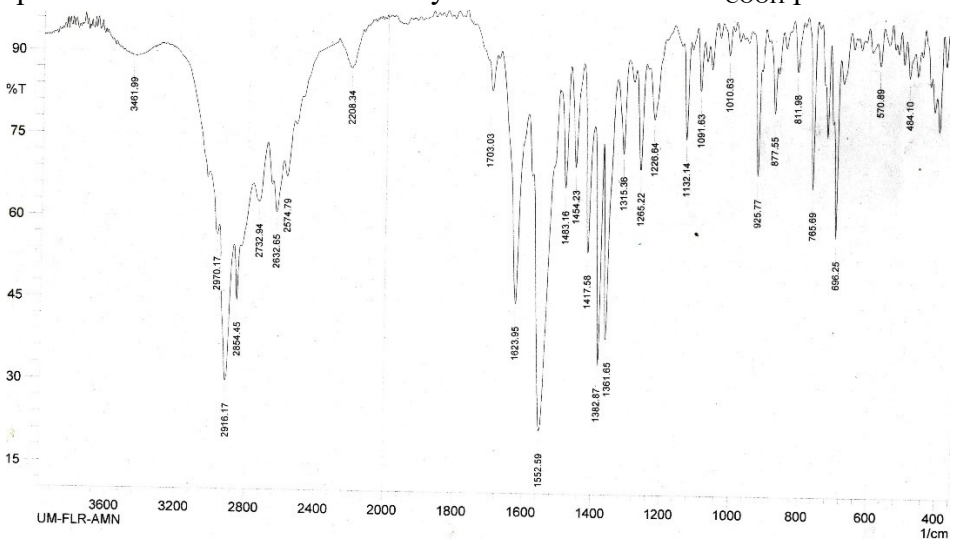

Figure S27: FT-IR spectra of **FLR·AMN** multidrug salt with the presence of charcteristic >C=O_{COO-} peak at 1623.95 cm^{-1} followed by the absense of >C=O_{COOH} peak.

Table S1: Gelation data table of multidrug salts studied herein:

Gelation Solvents	FLR-PHE-MAF	FLR-PHE-AMN	FLR-ALA-MAF	FLR-ALA-AMN	FLR-MAF	FLR-AMN
Bromobenzene	WG	GP	GP	GP	GP	**GEL**
Chlorobenzene	WG	GP	WG	INS	GP	WG
1,2-Dichlorobenzene	WG	CF	GP	GP	GP	WG
Toluene	**GEL**	WG	INS	INS	GP	GP
o-Xylene	WG	**GEL**	WG	WG	GP	WG
m- Xylene	WG	**GEL**	WG	GP	GP	GP
p- Xylene	WG	**GEL**	WG	GP	GP	WG
Mesitylene	GP	WG	INS	WG	GP	WG
Nitrobenzene	GP	**GEL**	GP	WG	GP	**GEL**
Methyl salicylate	WG	**GEL** (2.5[a], 94-95°C[b])	PS	GP	WG/CF	**GEL**
Water	**GEL** (3.5, 80-82°C[b])	WG	INS	INS	INS	INS

Note: [a]MGC, [b]T_{Gel}, WG: weak gel, GP: gelatinous precipitate, CF: crystalline fibre, INS: insoluble, PS: partially soluble.

Table S2: tanδ value table of hydrogel and all the organogels of multidrug salts under study:

Gels	G' (KPa)	G" (KPa)	tanδ
FLR·PHE·MAF-HG	5.95	1.63	0.27
FLR·PHE·MAF-TOL	1.28	0.40	0.31
FLR·PHE·AMN-MS	90.32	12.05	0.13
FLR·PHE·AMN-NB	6.83	1.65	0.24
FLR·PHE·AMN-OXY	8.92	1.19	0.13
FLR·PHE·AMN-MXY	35.25	4.96	0.14
FLR·PHE·AMN-PXY	8.81	1.45	0.16
FLR·AMN-MS	0.73	0.40	0.23
FLR·AMN-NB	5.29	1.48	0.28
FLR·AMN-BB	3.41	1.01	0.30

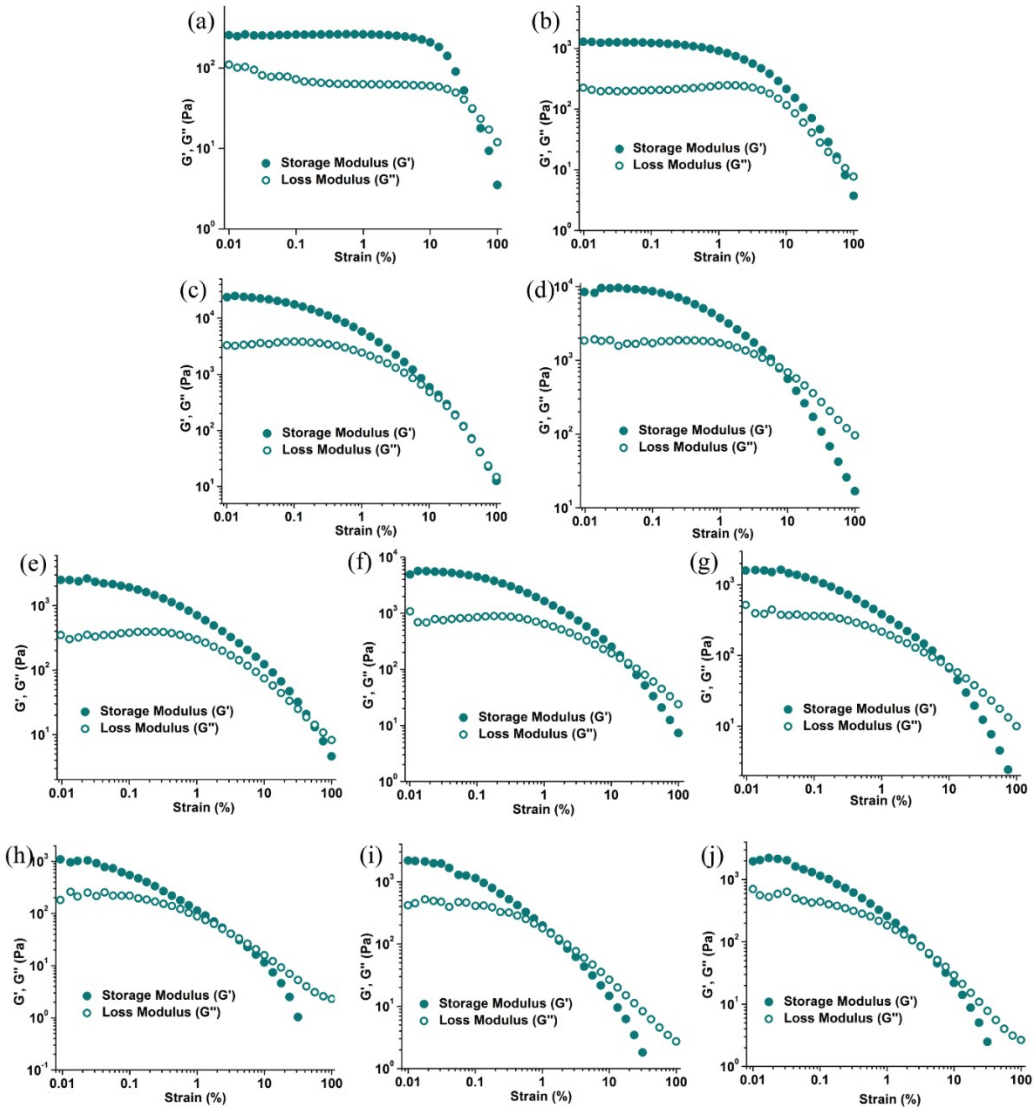

Figure S28: Strain sweep or amplitude sweep plots of all the gels under study (a) **FLR-PHE-MAF-HG**, (b) **FLR-PHE-MAF-TOL**, (c) **FLR-PHE-AMN-MS**, (d) **FLR-PHE-AMN-NB**, (e) **FLR-PHE-AMN-OXY**, (f) **FLR-PHE-AMN-MXY**, (g) **FLR-PHE-AMN-PXY**, (h) **FLR AMN-MS**, (i) **FLR-AMN-NB** and (j) **FLR-AMN-BB**.

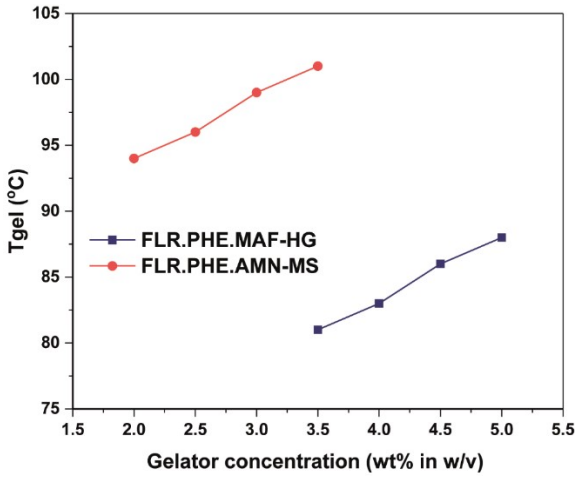

Figure S29: T_{gel} *vs* [gelator] plot of **FLR-PHE-MAF-**HG and **FLR-PHE-AMN-**MS**.**

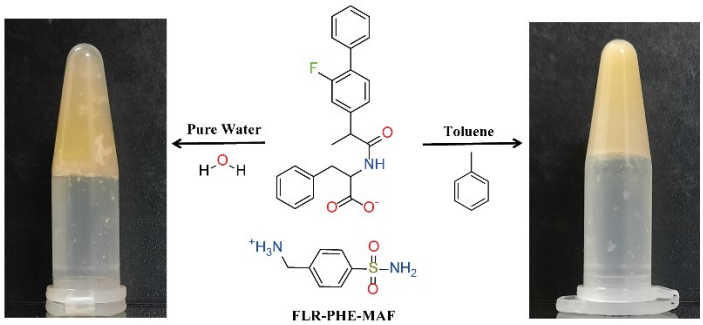

Figure S30: Optical images of pure hydrogel and toluene gel of **FLR·PHE·MAF** multidrug.

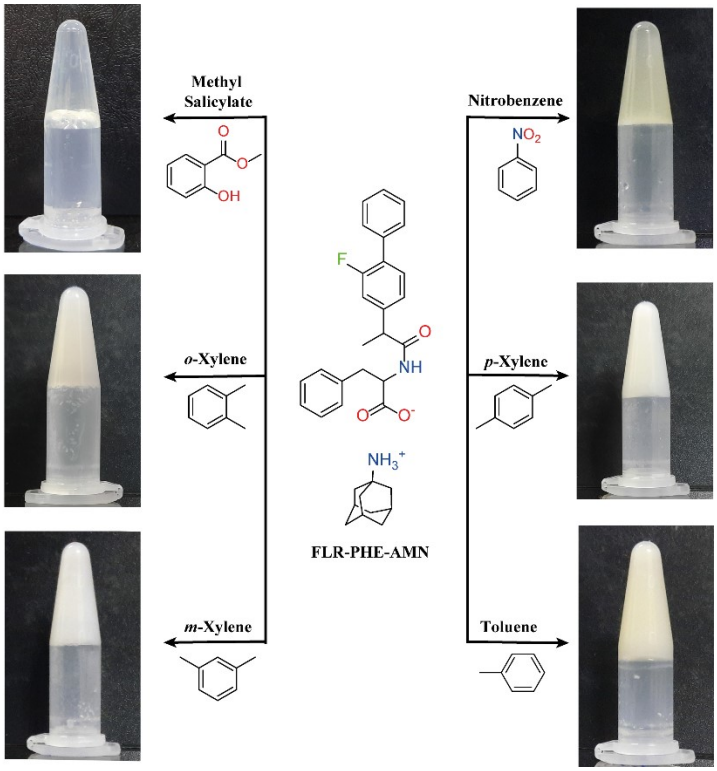

Figure S31: Optical images of MS and other organogels of **FLR·PHE·AMN** multidrug.

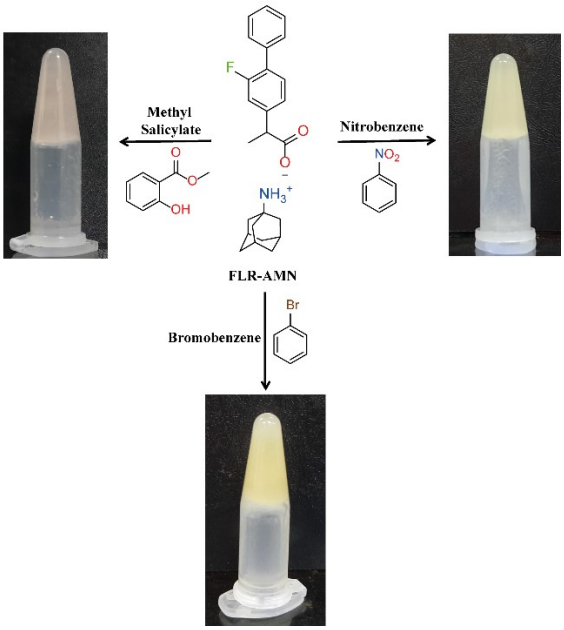

Figure S32: Optical images of MS and other organogels of **FLR·AMN** multidrug.

Table S3: Crystallographic data parameters for the single crystal of **FLR·AMN** salt:

Parameters	**FLR·AMN**
CCDC No.	2192760
Empirical formula	$C_{25}H_{30}FNO_2$
Formula weight	395.50
Temperature/K	145.15
Crystal system	orthorhombic
Space group	$P2_12_12_1$
a/Å	6.3673(13)
b/Å	16.941(3)
c/Å	19.629(4)
α/°	90
β/°	90
γ/°	90
Volume/Å^3	2117.3(7)
Z	4
ρ_{calc}g/cm^3	1.241
μ/mm^{-1}	0.084
F(000)	848.0
Crystal size/mm^3	0.12 × 0.03 × 0.02
Radiation	MoKα (λ = 0.71073)
2Θ range for data collection/°	4.796 to 49.994
Index ranges	$-7 \leq h \leq 7$, $-20 \leq k \leq 19$, $-23 \leq l \leq 23$
Reflections collected	19709
Independent reflections	3739 [R_{int} = 0.1071, R_{sigma} = 0.0825]
Data/restraints/parameters	3739/1/261
Goodness-of-fit on F^2	1.198
Final R indexes [I>=2σ (I)]	R_1 = 0.1653, wR_2 = 0.3936
Final R indexes [all data]	R_1 = 0.2053, wR_2 = 0.4309
Largest diff. peak/hole / e Å^{-3}	1.30/-0.55

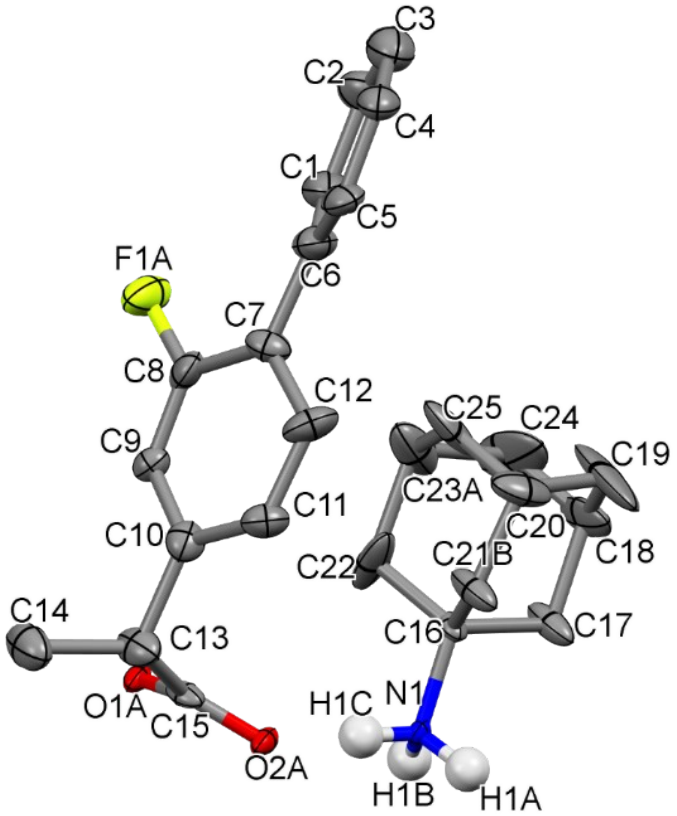

Figure S33: ORTEP-plot of **FLR·AMN** multidrug salt bearing H-atoms participating hydrogen bond network formation.

Table S4: Hydrogen-bond data table for the single crystal of **FLR·AMN** salt:

Bisamide	D-H•••A	*d*(D-H) (Å)	*d*(H•••A) (Å)	*d*(D•••A) (Å)	∠D–H•••A (°)	Symmetry operator
FLR·AMN	N1-H1A•••O1A	0.91	1.90	2.782(14)	163	-1/2+x,3/2-y,2-z
	N1-H1A•••O1B	0.91	2.05	2.880 (2)	151	-1/2+x,3/2-y,2-z
	N1-H1B•••O2A	0.91	1.91	2.793 (15)	162	1/2+x,3/2-y,2-z
	N1-H1B•••O2B	0.91	1.83	2.686(19)	155	1/2+x,3/2-y,2-z
	N1-H1C•••O2A	0.91	1.90	2.782(14)	164	-1+x,y,z
	N1-H1C•••O1B	0.91	1.86	2.750 (2)	165	-1+x,y,z

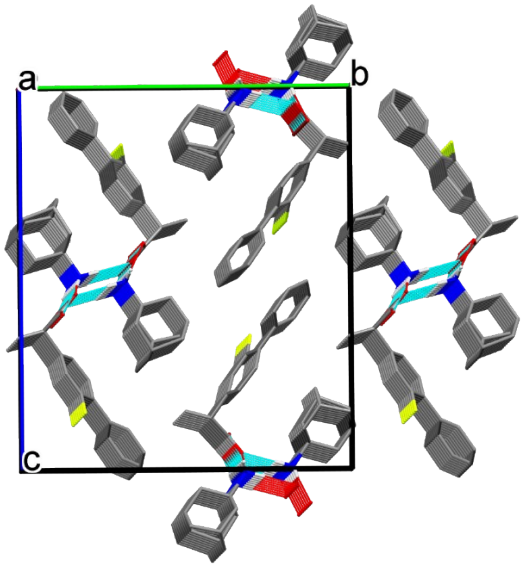

Figure S34: Packing diagram of **FLR·AMN** multidrug salt as viewed along crystallographic *b* axes.

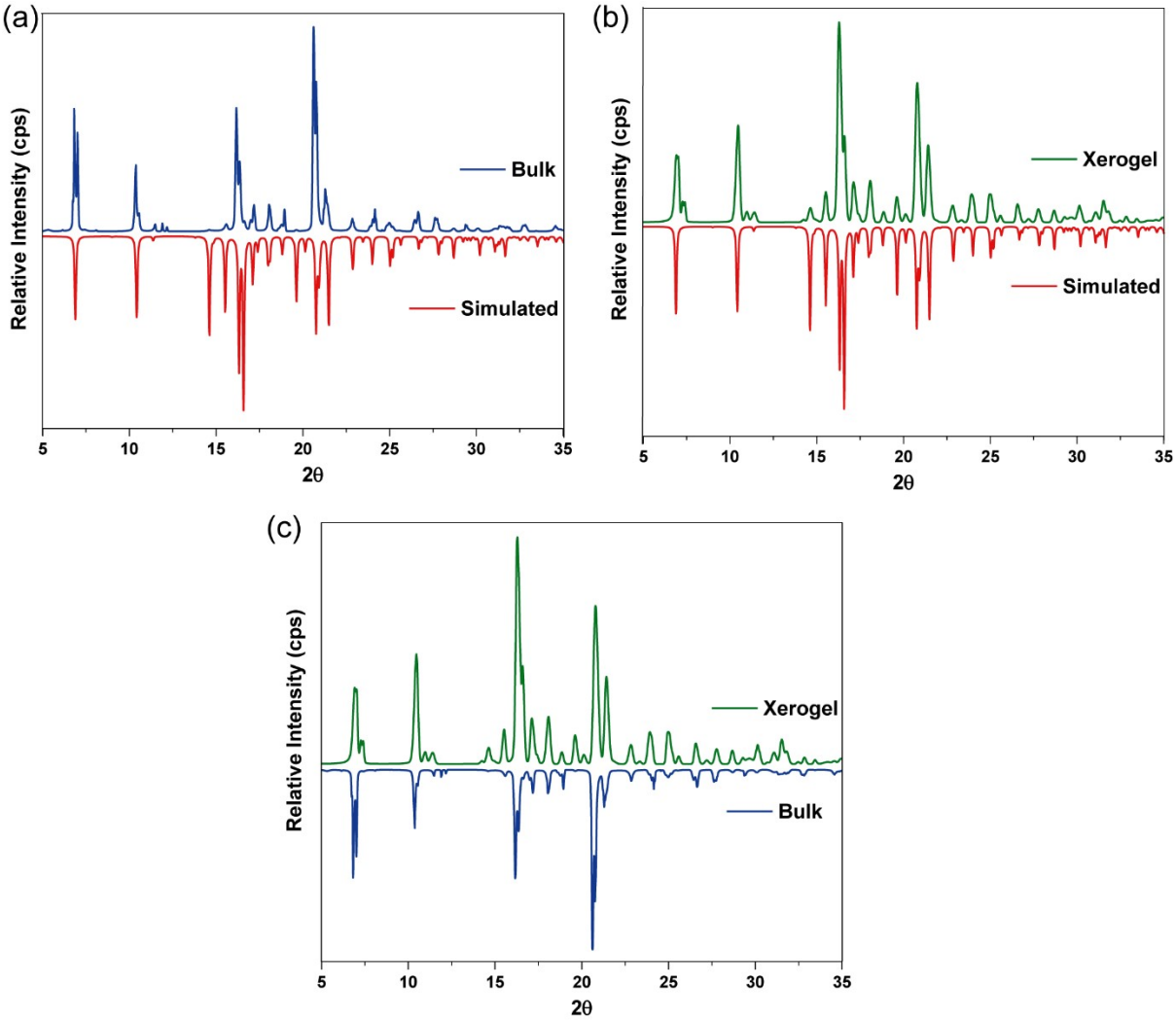

Figure S35: Comparative X-ray powder diffraction patterns of the gelator **FLR·AMN**; (a) simulated-bulk, (b) simulated-xerogel and (c) xerogel-bulk

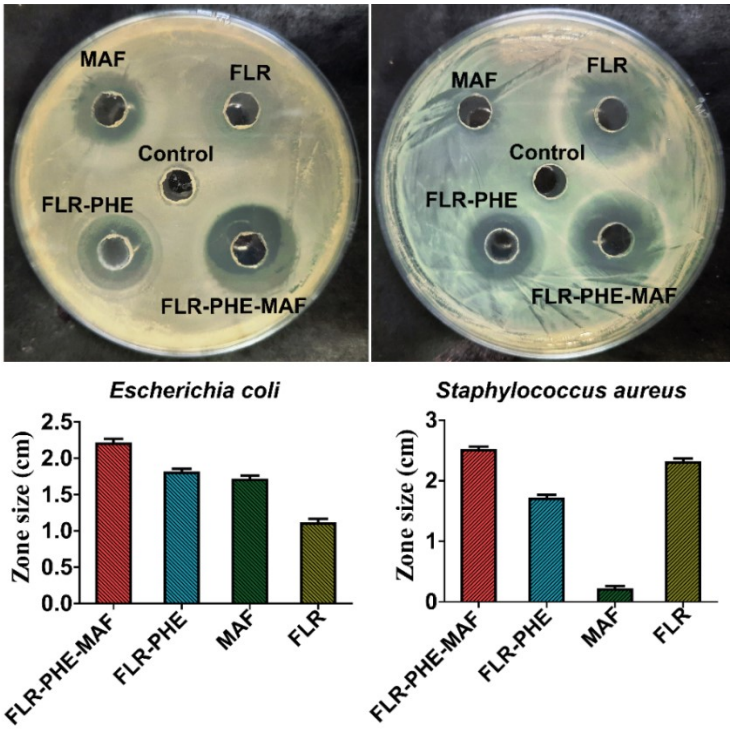

Figure S36: Antibacterial zone inhibition assay different components of multidrug hydrogelator salt **FLR·PHE·MAF** studied herein against *E. coli* and *S. aureus* bacteria.

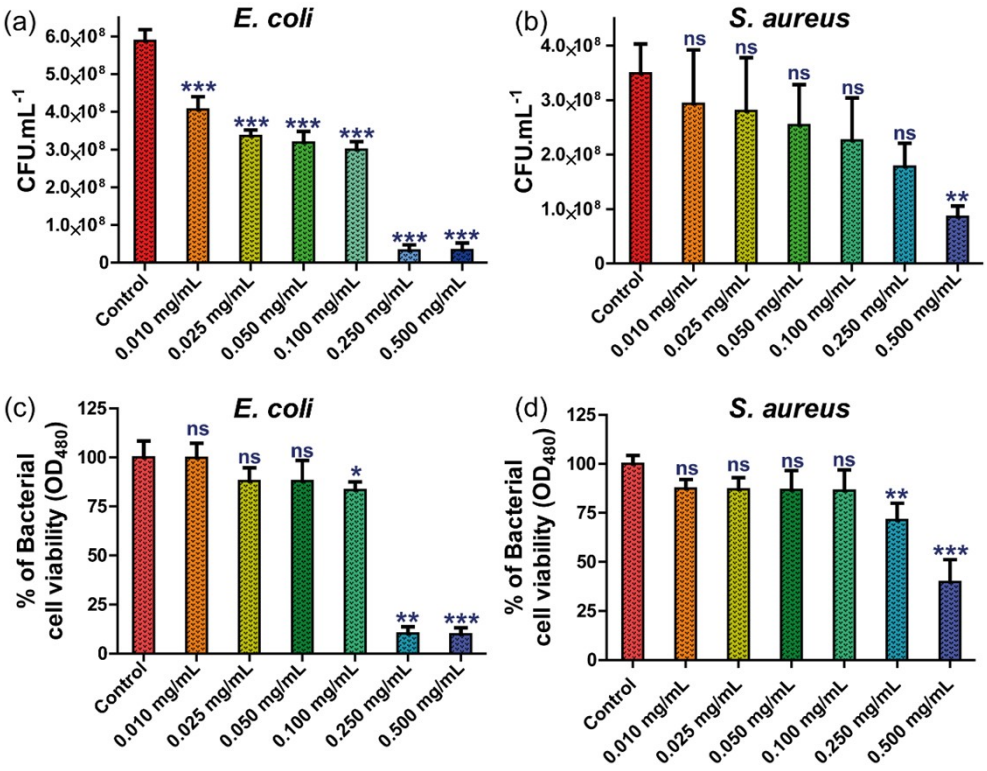

Figure S37: Antibacterial activity (turbidity assay at OD_{600}) of multidrug hydrogelator salt **FLR·PHE·MAF** against (a) *E. coli* and (b) *S. aureus* bacteria; and antibacterial activity (INT assay at OD_{480}) of multidrug hydrogelator salt **FLR·PHE·MAF** against (c) *E. coli* and (d) *S. aureus*. Data are represented considering mean ± SD where *P < 0.05, **P < 0.01, ***P < 0.001, and ns represents not significant.

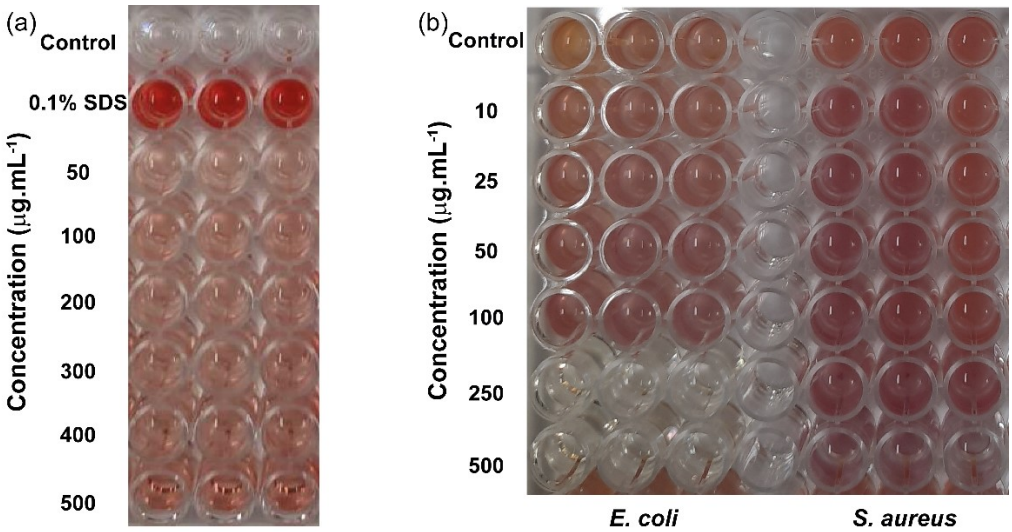

Figure S38: Optical images showing the activity of multidrug hydrogelator salt **FLR·PHE·MAF** (a) in haemolysis study to check cytocompatibility in living systems and (b) INT assay at different concentration of the multidrug to determine the MIC range against two bacteria.